

Cite this: *J. Mater. Chem. B*, 2018, 6, 740

## Mesoporous silica nanoparticles/gelatin porous composite scaffolds with localized and sustained release of vancomycin for treatment of infected bone defects†

Xiaojun Zhou,<sup>‡</sup> Weizong Weng,<sup>‡</sup> Bo Chen,<sup>c</sup> Wei Feng,<sup>a</sup> Weizhong Wang,<sup>a</sup> Wei Nie,<sup>a</sup> Liang Chen,<sup>a</sup> Xiumei Mo,<sup>‡</sup> Jiacan Su<sup>‡</sup>\*<sup>b</sup> and Chuanglong He<sup>‡</sup>\*<sup>a</sup>

Treatment of infected bone defects still remains a formidable clinical challenge, the design of bone implants with the controlled release of antibiotics is now regarded as a powerful strategy for infection control and bone healing. In this study, we fabricated a composite scaffold based on vancomycin (Van) loaded mesoporous silica nanoparticles (Van@MSNs) and a gelatin matrix. The microscopic structure of the gelatin-based composite scaffolds was characterized as highly porous. By the addition of MSNs, an enhancement in the compression property of MSNs-incorporated composite scaffolds was observed. The Van could release from the Van@MSNs incorporated composite scaffold in a sustained-release manner with a minimal burst, and thus effectively inhibit the growth of *Staphylococcus aureus* in a subsequent *in vitro* antibacterial study. In addition, the drug-loaded composite scaffold showed no unfavorable effects on the proliferation and differentiation of bone mesenchymal stem cells (BMSCs), confirming good biocompatibility. Moreover, *in vivo* results demonstrated that the antibiotic-loaded composite scaffold could significantly reduce bacterial contamination while promoting bone healing. Thus, our results suggest that the fabricated Van@MSNs/Gelatin composite scaffold with a localized and sustained release of antibiotics is a promising biomaterial for treating infected bone defects.

Received 8th May 2017,  
Accepted 4th January 2018

DOI: 10.1039/c7tb01246b

rsc.li/materials-b

### 1. Introduction

Bone defect-related infections that result from severe bone trauma and open fracture continue to be a troublesome problem in orthopedic clinics. Owing to the presence of infection, patient outcomes were found to be dramatically affected, especially experiencing delayed bone union and partial amputation.<sup>1</sup> It is because bone defects with infections often cause limited blood supply in the infected sites, thus resulting in a poor ability to self-heal and restore the structure and function of bone tissue.<sup>2</sup> Therefore, antibacterial agents loaded into the bone implants for treating infected bone defects are required.<sup>3,4</sup> To reduce or eradicate the contaminations by infections, significant studies

have focused on the development of bone repair materials with a local antibiotics delivery capability.<sup>5–8</sup>

Generally, the antibacterial drugs tend to be loaded into the implants by simple adsorption for eliminating infection. In this case, local delivery of antibiotics in the infected area can be easily realized through local implantation of antibiotic-laden materials.<sup>9</sup> Meanwhile, it has been indicated that the controlled release of antibiotics from implanted scaffolds is more desirable since this can afford the effective antibacterial concentration in a sustained release pattern.<sup>7,10</sup> Furthermore, this drug release manner is deemed to be available to meet the requirements of long-term bacterial inhibition and tissue regeneration.<sup>11,12</sup> Therefore, a drug-loaded composite scaffold, which can maintain sustained drug release locally, is promising for clinical treatment.

Up to now, many strategies have been developed to enable the controlled release of loaded drugs in the scaffolds. Among them, the integration of drug-loaded microcarriers into polymer matrices is generally accepted as a prominent strategy for optimizing the drug release profile.<sup>13,14</sup> To serve as the microcarriers, numerous organic and inorganic particles have been used, such as poly (lactic-co-glycolic) acid (PLGA) microparticles,<sup>15</sup> nano-hydroxyapatite<sup>16</sup> and silica nanoparticles.<sup>17</sup> Specially, mesoporous

<sup>a</sup> College of Chemistry, Chemical Engineering and Biotechnology, State Key Laboratory for Modification of Chemical Fibers and Polymer Materials, Donghua University, Shanghai 201620, P. R. China. E-mail: hcl@dhu.edu.cn

<sup>b</sup> Department of Orthopaedics Trauma, Changhai Hospital, Second Military Medical University, Shanghai 200433, P. R. China. E-mail: dr\_sujiacan@163.com

<sup>c</sup> Department of Radiology, Shanghai East Hospital, Tongji University School of Medicine, Shanghai 200120, P. R. China

† Electronic supplementary information (ESI) available. See DOI: 10.1039/c7tb01246b

‡ These authors contributed equally to this paper.

silica nanoparticles (MSNs) have been employed as potential nano-additives in tissue engineering because of their unique advantages, including controllable particle size and pore size and high drug loading capacity, as well as an excellent biocompatibility.<sup>18,19</sup> Moreover, MSNs have been incorporated into polymer materials to increase their mechanical properties, improve cell adhesion and proliferation and enhance the osteogenic differentiation of osteoblasts.<sup>20,21</sup> Importantly, drug release from the MSN-incorporated composite scaffolds can be well controlled.<sup>13,22</sup> Inspired by these superior performances, the integration of polymer scaffolds and MSNs might be a powerful strategy to construct controlled delivery system for bone regeneration.

For bone tissue engineering applications, a porous scaffold has natural advantages over a dense one, and could realize a proper oxygen/nutrient delivery, tissue ingrowth as well as neovascularization because of the open space and high surface area.<sup>23</sup> Gelatin is a biocompatible macromolecule derived from collagen; therefore, the contained Arg-Gly-Asp (RGD) sequences make it promote cell attachment, cell spreading and proliferation.<sup>24,25</sup> Compared with other polymers used in scaffold preparation, gelatin has gained much attention for 3D porous scaffold fabrication in tissue engineering owing to its availability, low immunogenicity, easy handling and that it is inexpensive.<sup>25</sup> In addition, the poor mechanical properties of gelatin-based scaffolds can be further improved by crosslinking and combining with inorganic compounds, thereby making it possible for them to become appropriate constructs for bone regeneration.<sup>26</sup> For example, nano-hydroxyapatite was the most frequently used constituent to fabricate the composite scaffold for bone tissue engineering.<sup>25,27</sup>  $\beta$ -tricalcium phosphate ( $\beta$ -TCP) had also been incorporated into the gelatin sponges for releasing the osteogenic growth factor to enhance bone regeneration.<sup>28</sup> Moreover, the silica nanoparticles were applied to the composite with gelatin to form a macroporous scaffold, which displayed favorable mechanical properties and bioactivity and showed attractive prospects as artificial bone grafting materials.<sup>29</sup> To meet the demand for inhibiting bacterial contamination, gelatin was combined with nanosilver to prepare the antibacterial macroporous scaffolds.<sup>30</sup> Furthermore, the gelatin/ $\beta$ -TCP composite scaffold was prepared for the controlled release of vancomycin.<sup>11</sup> The result showed that the vancomycin-loaded composite scaffolds could allow a local therapeutic drug concentration over an extended duration, which showed a good vancomycin delivery system for potential application in the treatment of osteomyelitis. However, further *in vivo* studies of those antibacterial composite scaffolds are still required to evaluate the therapeutic effects. To the best of our knowledge, there is no report on the preparation of MSNs/gelatin composite scaffolds for local vancomycin delivery in infected bone defect treatment. Therefore, given the prominent advantages of them, we hypothesize that gelatin combined with MSNs will be good candidates for the controlled release of vancomycin in infection control and bone defect repair. Moreover, a systemic study regarding to biocompatibility, osteogenic potential and inhibition effects on bacterial growth of this constructed

release system is intended to be performed both *in vitro* and *in vivo*.

Herein, a composite scaffold composed of gelatin matrix and vancomycin-loaded MSNs was developed for treating infected bone defects. The influence of MSNs on the morphology and mechanical properties of the composite scaffolds was studied. The drug release profiles, antibacterial effect against *Staphylococcus aureus*, proliferation and differentiation of bone mesenchymal stem cells (BMSCs) on the composite scaffolds were also investigated. Finally, *in vivo* tests of repair efficacy on the infected bone defects were evaluated using micro-computed tomography (micro-CT) examination and histological analysis.

## 2. Materials and methods

### 2.1 Materials

Gelatin from bovine skin (type B, ~225 g Bloom), tetraethyl orthosilicate (TEOS), cetyltrimethylammonium bromide (CTAB), 1-ethyl-3(3-dimethylaminopropyl) carbodiimide hydrochloride (EDC) and *N*-hydroxysuccinimide (NHS) were purchased from Sigma-Aldrich Trading Co., Ltd (Shanghai, China). Vancomycin hydrochloride (Van) was obtained from Aladdin Chemistry, Co., Ltd (Shanghai, China). Calcein-AM, TRIeasy total RNA extraction reagent, Hieff™ first strand cDNA synthesis kit and Hieff™ qPCR SYBR Green Master Mix (Low Rox Plus) Kit were purchased from Yeasen Biotechnology Co., Ltd (Shanghai, China). The water used in all the experiments was purified using a Milli-Q water purification system (Millipore, Bedford, MA) with a resistivity higher than 18.2 M $\Omega$  cm. All other chemicals were of analytical grade from Sinopharm Chemical Reagent Co., Ltd (Shanghai, China).

### 2.2 Fabrication of MSNs

Briefly, 0.5 g of CTAB was dissolved in 240 mL of deionized water, and then 0.14 g of NaOH was added into the above solution. After the solution was stirred vigorously at 80 °C for 2 h, 2.5 mL of TEOS was introduced dropwise. The mixture solution was allowed to stir for another 2 h and then subjected to centrifugation (8000 rpm, 10 min) to collect the white product. The obtained product was washed several times with deionized water and ethanol. After that, the product was suspended in a solution of 9 mL of HCl and 160 mL of ethanol and then extracted at 80 °C for 24 h to remove the surfactant CTAB. The extraction was repeated three times. Finally, the surfactant-removed MSNs were obtained by centrifugation and dried by lyophilization.

### 2.3 Van loading in MSNs

For Van loading, 20 mg of Van was added into the 4 mL of MSN dispersion solution (25 mg mL<sup>-1</sup>) in deionized water. The mixture was stirred at room temperature in dark conditions for 4 h, and then settled in a vacuum oven under vacuum treatment for another 2 h to facilitate the drug encapsulation into the channel of the MSNs. The Van-loaded MSNs dispersion solution was taken out and treated by centrifugation.

Subsequently, the collected Van-loaded MSNs (Van@MSNs) were washed twice with deionized water. To determine the drug loading capacity, the supernatant and washing solution were collected and measured by a UV-vis spectrophotometer (JASCO V530, JASCO, Japan) at a wavelength of 280 nm. The loading content of Van in Van@MSNs was calculated according to the following equation. The loading content was calculated to be 7.4 wt%.

$$\text{Loading content (\%)} = \frac{\text{weight of loaded drug}}{\text{weight of drug loaded nanocarrier}} \times 100\%$$

#### 2.4 Preparation of composite scaffolds

To prepare the scaffolds, 800 mg of gelatin powder was first dissolved in 9 mL of deionized water at 40 °C. After the gelatin had dissolved completely, 1 mL of MSNs or Van@MSNs stock solution was added. The resulting mixture was stirred vigorously to make a homogeneous solution. After that, the mixture solution was gently introduced into the mold with no bubbles inside. The gel was formed after being kept at 4 °C for 1 h, and then transferred to -20 and -80 °C sequentially. When the gel was completely frozen, the gelatin matrices were then lyophilized to obtain the scaffolds. In order to investigate the influence of MSNs on the physical properties of the scaffolds, composite scaffolds containing different MSNs contents (5, 10 and 20 wt% relative to gelatin) were fabricated, and they are denoted as 5% MSNs/Gelatin, 10% MSNs/Gelatin and 20% MSNs/Gelatin. A pure Gelatin scaffold and a Van-loaded Gelatin (Van@Gelatin) scaffold were also fabricated to be used as the controls. Subsequently, the dried scaffolds were crosslinked using EDC and NHS in a mixture solvent of acetone/water (v/v = 4:1) at 4 °C for 24 h. Then the crosslinked scaffolds were washed more than 3 times with deionized water and freeze-dried under vacuum for 3 days. Finally, the dried gelatin-based porous scaffolds were obtained and stored in centrifuge tubes at -20 °C for later use.

#### 2.5 Characterization

The structure of the MSNs was observed with a transmission electron microscope (JEM-2100F, Jeol Ltd, Japan) operating at 200 kV. The size distribution of the prepared nanoparticles was determined by dynamic light scattering (DLS) using a BI-200SM multi-angle dynamic/static laser scattering instrument (Brookhaven, USA). The surface area and pore size distribution of the MSNs were obtained by the Brunauer-Emmett-Teller (BET) and Barrett-Joyner-Halenda (BJH) methods from N<sub>2</sub> adsorption-desorption isotherm measurements (V-Sorb 2800P analyzer, Gold APP, China). The surface morphologies of the scaffolds were visualized with a scanning electron microscope (TM-1000, Hitachi, Japan). The average pore diameter in each scaffold was measured using SEM images with Image J 1.34 software, with at least 100 measurements of the pores randomly selected. Attenuated total reflectance-Fourier transform infrared (ATR-FTIR) spectra were conducted with a Nicolet 6700 spectrometer (Thermo, USA) at a resolution of 1 cm<sup>-1</sup> in the range of 400–4000 cm<sup>-1</sup>. The mechanical properties of the scaffolds were recorded using a mechanical tester (HY-940FS, Shanghai Hengyu Co., Ltd,

China) with a 200 N load cell. A loading rate of 1 mm min<sup>-1</sup> was used for all cylindrical samples (diameter, 10 mm; thickness, 8 mm). Three replicates were carried out for each group.

#### 2.6 In vitro drug release

The drug release profile from the Van-loaded MSNs/Gelatin (Van@MSNs/Gelatin) scaffold was investigated. As a control, the release property of the Van-loaded Gelatin scaffold was also evaluated. First, 50 mg of each scaffold was weighed and immersed into 4 mL of PBS solution (pH = 7.4) in the centrifuge tube. Then the tubes were incubated in a thermostatic shaker at 37 °C with a speed of 100 rpm. 2 mL of the released medium was taken out at the selected time intervals and supplemented with an equal volume of fresh PBS solution. Following a standard calibration curve of Van in the PBS solution, the concentration of released Van in the medium at each time point was determined using an UV-vis spectrophotometer at a wavelength of 280 nm.<sup>9</sup> Finally, the cumulative release percentage of Van from the scaffold was calculated with three parallel samples.

#### 2.7 In vitro antibacterial activity assay

In this work, *Staphylococcus aureus* (*S. aureus*), a Gram-positive bacterium, was selected to evaluate the antibacterial activity of fabricated scaffolds. The antibacterial activity experiments were carried out by both quantitative and qualitative analyses. For the quantitative analysis, the frozen *S. aureus* was first activated with a liquid medium of trypticase soy broth (TSB) at 37 °C in an oscillation incubator with a speed of 120 rpm. Afterward, the activated *S. aureus* was introduced into each test tube with 5 mL of TSB liquid medium, which was fixed at an OD value of 0.1–0.2 at 625 nm. The scaffolds were sterilized with ultraviolet radiation before usage. Then, the TSB medium containing *S. aureus* in each test tube was respectively incubated with Gelatin, MSNs/Gelatin, Van@Gelatin, Van@MSNs/Gelatin and free Van with the equivalent Van concentrations ranging from 0 to 60 µg mL<sup>-1</sup> (Van content in each sample relative to the bacterial suspension). The bacterial solution without any treatment was performed as the control and each group was conducted with three parallel samples. After that, the mixture was incubated at 37 °C with shaking at 120 rpm for 24 h. The absorbance in each group was then monitored with a UV-vis spectrophotometer at 625 nm. Finally, the percentage of bacterial inhibition was calculated using the following equation.

$$\text{Bacterial inhibition (\%)} = \frac{A_{\text{Control}} - A_{\text{Test}}}{A_{\text{Control}}} \times 100\%$$

where  $A_{\text{Control}}$  and  $A_{\text{Test}}$  are the OD values of the control group and the test group, respectively. Additionally, the antibacterial activity of Van@Gelatin and Van@MSNs/Gelatin scaffolds (with an original Van content of 60 µg mL<sup>-1</sup> in 5 mL medium) after different drug release time periods (3, 7 or 13 days) was also investigated under similar conditions.

For qualitative analysis, the antibacterial activity of scaffolds was observed *via* the inhibition zone of the *S. aureus*. Typically,

the *S. aureus* suspended in a TSB medium (100  $\mu\text{L}$ ) was first spread onto the agar plates. Then sterilized circular scaffolds (Gelatin, MSNs/Gelatin, Van@Gelatin and Van@MSNs/Gelatin) with diameters of approximately 10 mm and a thickness of 1 mm were placed onto the agar plate. After incubation at 37  $^{\circ}\text{C}$  for 12 and 24 h, the images of the inhibition zone on the plate were captured using an automatic colony counter (Hangzhou Shineso Science & Technology, China). The inner and outer diameters of the inhibition zone were also accurately measured using the same instrument. Furthermore, the antibacterial activity of the Van@Gelatin and Van@MSNs/Gelatin circular scaffolds after a 3, 7 or 13 day release period was also investigated under similar conditions.

## 2.8 Cell adhesion and proliferation on the scaffolds

BMSCs were isolated from the femurs of SD rats and cultured in DMEM/F-12 supplemented with 10% FBS, 100  $\text{U mL}^{-1}$  penicillin, and 100  $\mu\text{g mL}^{-1}$  streptomycin at 37  $^{\circ}\text{C}$  in a humidified incubator with 5%  $\text{CO}_2$ .<sup>17</sup> Before cell seeding, all the scaffolds were cut into cylinders with a diameter of 10 mm and thickness of 1 mm, and then sterilized with fumigation in 75% ethanol for 24–48 h and subsequent ultraviolet radiation for 6 h. To evaluate the BMSCs proliferation on the scaffolds, a live cell staining using calcein-AM (Yeasen Biotechnology Co., Ltd, Shanghai, China) and a cell counting kit-8 assay (CCK-8, Beyotime, China) were carried out. Briefly, BMSCs were seeded on the scaffolds in 48-well plates at a cell density of  $2 \times 10^4$  per well and cultured for different time points. For cell adhesion evaluation, the cells were washed with PBS after being cultured for 6 and 12 h, and then incubated with a calcein-AM working solution (2  $\mu\text{M}$ , 200  $\mu\text{L}$ ) for 0.5–1 h. After being washed with PBS, the cells with green fluorescence were imaged using an inverted fluorescence microscope (IX71, Olympus, Japan). After the cells were cultured on the scaffolds for 2, 4 and 7 days, the medium was replaced with a prepared CCK-8 working solution (200  $\mu\text{L}$ ). 100  $\mu\text{L}$  of the supernatant in each well was taken out and transferred into a 96-well plate after 1 h incubation. Then the absorbance was read with a microplate reader (Multiskan GO, Thermo, USA) at 450 nm. The cell viability of each group was expressed as the percentage of the experiment group to the control group. For fluorescence observation, live cell staining was also performed for the same culture periods (2, 4 and 7 days).

## 2.9 Osteogenic differentiation evaluation *in vitro*

The *in vitro* osteogenic differentiation of BMSCs on scaffolds was investigated by alkaline phosphatase (ALP) activity and osteo-related gene expression determination. For the ALP activity measurement, BMSCs were seeded on the scaffolds in 24-well plates at a density of  $1 \times 10^5$  cells per well, and cultured for 24 h to allow the cell attachment. Afterward, the medium was changed with an osteogenic medium (DMEM/F-12 medium supplemented with 50  $\mu\text{g mL}^{-1}$  L-ascorbic acid, 10 mM  $\beta$ -glycerol phosphate and  $10^{-8}$  M dexamethasone). Then the culture of the cells was continued to for 7 and 14 days. At different time points, the cells were washed with PBS and then lysed with cell lysis buffer.

After centrifugation, 50  $\mu\text{L}$  of the supernatant was collected to measure the ALP activity using an Alkaline Phosphatase Assay Kit (Beyotime, China). For normalization, the total protein concentration of each sample was detected using a BCA Protein Assay Kit (Beyotime, China).

When the cells were cultured on scaffolds for 7 and 14 days, the mRNA expression of the osteo-related gene was measured by quantitative real time PCR (qRT-PCR), including runt-related transcription factor 2 (RUNX2), osteopontin (OPN) and osteocalcin (OCN). First, the total RNA in each sample was extracted using TRIzol reagent (Invitrogen, USA) and the RNA concentration was determined using the NanoDrop 2000 spectrophotometer (Thermo Scientific, USA). Complementary DNA (cDNA) was then synthesized using a Hieff<sup>TM</sup> First Strand cDNA Synthesis Kit following the manufacturer's protocol. Subsequently, the target gene expression was analyzed on the 7500 Fast Real-time PCR System (Applied Biosystems) using a Hieff<sup>TM</sup> qPCR SYBR Green Master Mix (Low Rox Plus) Kit. The housekeeping gene, glyceraldehydes-3-phosphate-dehydrogenase (GAPDH), was used as internal control. The primer sequences for these genes are listed in Table S1 (ESI<sup>†</sup>).

## 2.10 *In vivo* animal experiments

### 2.10.1 Animal model establishment and scaffold implantation.

The feasibility of a Van-loaded MSNs/Gelatin scaffold for infected bone defect treatment was further investigated *in vivo*. The animal studies were performed in compliance with the NIH guidelines for the care and use of laboratory animals (NIH Publication No. 85-23 Rev. 1985) and approved by the ethics committee in animal experimentation of the Research Center for Laboratory Animal of the Second Military Medical University, Shanghai, China. To establish the infected bone defect model, male New-Zealand rabbits (2.5–3.0 kg) were purchased from Shanghai SLAC Laboratory Animal Co., Ltd (Shanghai, China). Before surgery, the initial white blood cell (WBC) data of all the rabbits were obtained from the marginal ear veins. After the rabbits were anesthetized using 3% pentobarbital sodium (30  $\text{mg kg}^{-1}$ ) through an intraperitoneal injection, the radius bone at the right forearm was carefully exposed. A segmental defect with a length of 10 mm in the middle of the radius shaft was created, followed by irrigation with a saline solution in the bone void. 0.5 mL of *S. aureus* suspension ( $2.5 \times 10^6$  CFU  $\text{mL}^{-1}$ ) and 0.2 mL of morrhuate sodium were then injected into the defect area and bone marrow cavity. After the surgery was completely finished, the rabbits were randomly assigned into three groups: A, Gelatin group; B, MSNs/Gelatin group and C, Van@MSNs/Gelatin group. At the predetermined time point, the WBC concentration in each group was monitored. At 2 weeks, the establishment of an infected bone defect model was further verified with Gram staining and Masson's trichrome staining. The detailed protocols are described in the ESI<sup>†</sup>.

After surgery for 14 days, the rabbits were anesthetized and the infected zone was treated with debridement, mimicking clinical practice. After that, the sterilized scaffolds (cut into 4 mm diameter, 10 mm thickness) were packed into the defects. The incision was sutured in a layered fashion and

wrapped with a sterile bandage. All the rabbits were then caged and allowed full activity postoperatively. For each group ( $n = 12$ ), the WBC concentration was also monitored weekly. Additionally, Van groups were also carried out in this study for comparison. Control 1 ( $n = 4$ ) were treated by a local injection of Van (equivalent Van content relative to Van@MSNs/Gelatin group) in the defect area and bone marrow cavity after debridement. Control 2 ( $n = 4$ ) were treated by debridement followed by a daily intravenous injection of Van (dose of  $6 \text{ mg kg}^{-1}$ ) for 4 weeks.<sup>31</sup> The specimens of the Van groups were finally harvested and evaluated at 12 weeks post-operation.

**2.10.2 Micro-CT measurement.** The *in vivo* bone regeneration on radius bone defects of rabbit was evaluated with a micro-CT scanner (SkyScan1076, Bruker micro-CT, Germany). At 4, 8 and 12 weeks post-operation, the rabbits were sacrificed with an overdose injection of 3% pentobarbital sodium. The bone tissue of interest was harvested by removing the attached fascia and muscular tissue, and the collected specimen was then evaluated by micro-CT. A 3D image for each specimen was reconstructed using the SkyScan CTVOX 2.1 software. The bone volume and bone mineral density within the defined region of interest (ROI) in the defect site were analyzed to quantify the amount of bone formation.

**2.10.3 Histological analysis.** For further evaluation of the bone formation, rabbits in each group were also sacrificed at 8 and 12 weeks. Then, the harvested bone tissue specimens were fixed in 4% paraformaldehyde, dehydrated in a graded series of ethanol, and embedded in polymethylmethacrylate. To observe new bone formation, sections of undecalcified specimens obtained by cutting and polishing were treated with hematoxylin and eosin (H&E) and toluidine blue (T-blue) staining. The stained sections were imaged using a light microscope (Nikon TE2000U, Japan).

### 2.11 Statistical analysis

The statistical analysis was performed using one-way analysis of variance (ANOVA), followed by *post hoc* Tukey's method to test all pair-wise mean comparisons. The results are expressed as mean  $\pm$  standard deviation. A value of  $*P < 0.05$  for all the tests was considered of statistical significance.

## 3. Results and discussions

The fabrication process of drug-loaded MSN-incorporated gelatin composite scaffold is schematically illustrated in Fig. 1. MSNs were prepared as reported previously and employed as microcarriers for loading the antibiotic Van. The Van-loaded MSNs and gelatin solutions were mixed together to obtain a homogeneous solution. The homogeneous solution obtained was then poured into the molds and treated with freeze-drying. After chemical crosslinking with EDC/NHS, the final product, a Van@MSNs/Gelatin porous scaffold, was produced *via* further lyophilization as expected.

### 3.1 Characterization of MSNs

The morphology and structural properties of the as-prepared MSNs were characterized by various techniques, including TEM observation, DLS and  $\text{N}_2$  adsorption-desorption measurements, as presented in Fig. S1 (ESI<sup>†</sup>). The TEM images in Fig. S1A (ESI<sup>†</sup>) show that the MSNs were spherical in particle shape with an ordered mesoporous structure. The hydrodynamic diameter of MSNs measured by DLS was 209.8 nm with a polydispersity index (PDI) of 0.152 (Fig. S1B, ESI<sup>†</sup>), which was slightly larger than that observed by TEM due to a hydration layer.<sup>32</sup>  $\text{N}_2$  adsorption-desorption isotherms and pore size distribution of the MSNs are displayed in Fig. S1C (ESI<sup>†</sup>). The isotherms exhibited the classical type-IV hysteresis, implying the presence of a well-defined mesoporous structure. Calculated by the BET and BJH methods, the surface area was  $833.5 \text{ m}^2 \text{ g}^{-1}$  and the size of the mesopore was centered at 2.4 nm, respectively. From these data, the advantages of a large surface area, uniform nano-scale particle size and pore size endowed the MSNs with highly desirable features to serve as carriers for drug loading.

### 3.2 Characterization of composite scaffolds

The microstructure of the MSNs/Gelatin composite scaffolds containing different contents of MSNs were observed by SEM images, as shown in Fig. 2. It is clearly seen that all of the MSNs/Gelatin composite scaffolds and pure Gelatin scaffold exhibited a highly porous structure. For the pure Gelatin scaffold, the pore wall surface was smooth and the pore diameter was

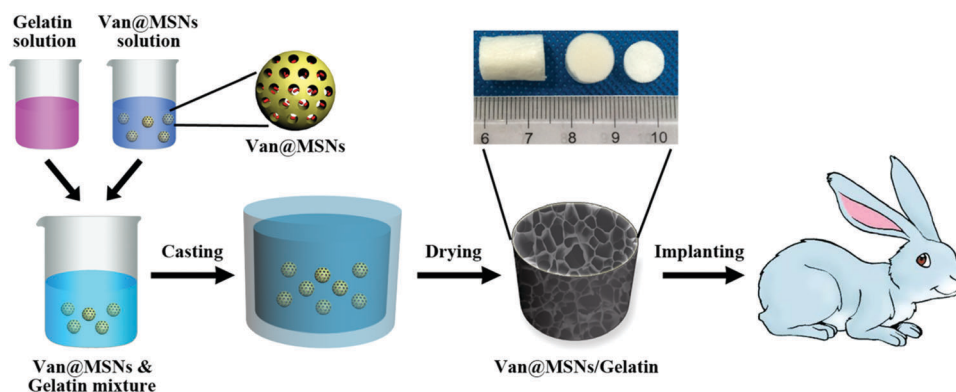


Fig. 1 Schematic illustration for the fabrication of the Van@MSNs/Gelatin composite scaffold.

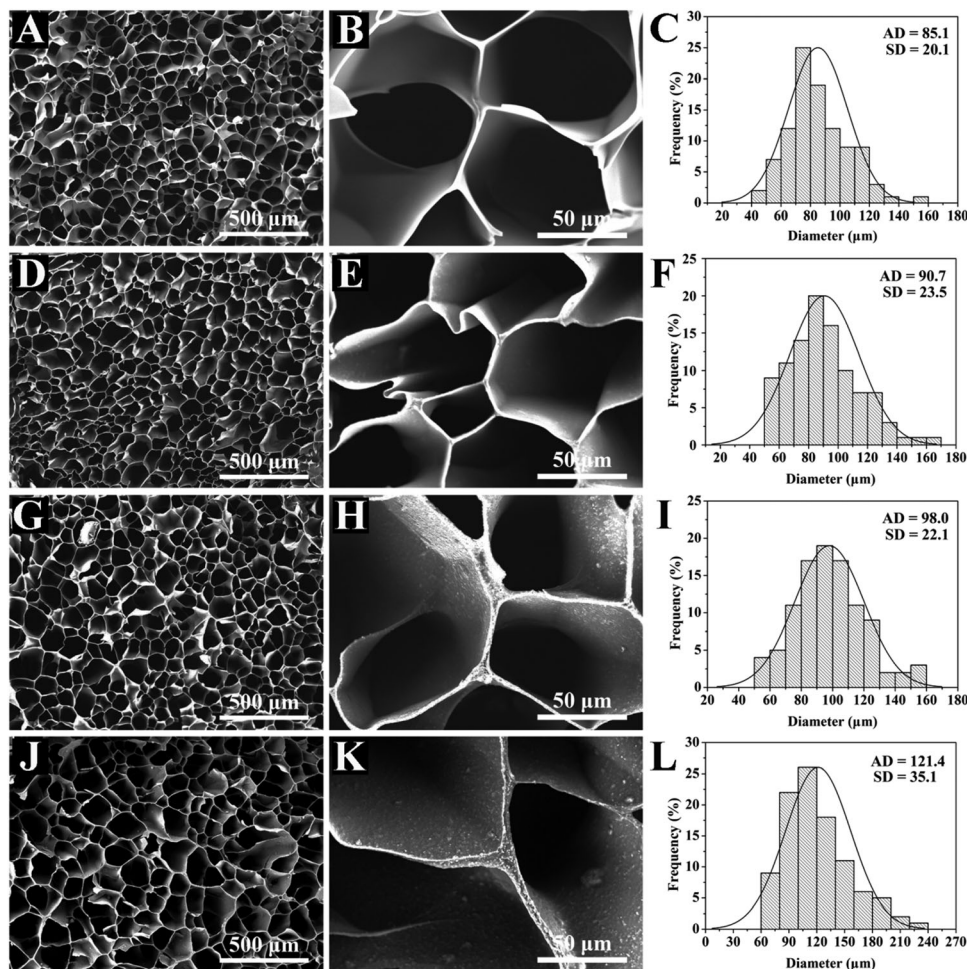


Fig. 2 SEM images of MSNs/Gelatin scaffolds with different contents of MSNs and their pore diameter distributions. (A–C) Pure Gelatin scaffold, (D–F) 5% MSNs/Gelatin scaffold, (G–I) 10% MSNs/Gelatin scaffold and (J–L) 20% MSNs/Gelatin scaffold. B, E, H and K are the magnified images corresponding to A, D, G and J, respectively.

calculated to be  $85.1 \pm 20.1 \mu\text{m}$ . However, an increase in the pore size ( $90.7 \pm 23.5$  to  $121.4 \pm 35.1 \mu\text{m}$ ) was observed when the content of the added MSNs was increased from 5 to 20% (Fig. S2, ESI<sup>†</sup>), and the pore size of the composite scaffolds with a 10% or 20% MSNs content was significantly larger than that of the Gelatin scaffold ( $P < 0.05$ ). Also, it was observed that the pore wall surface was rougher with the MSN content increasing in the MSNs/Gelatin composite scaffolds. When the introduced MSNs content was up to 20%, some obvious particle aggregates appeared, indicating an overload of MSNs within the gelatin matrix at the given amount. The result indicated that the fabricated MSNs/Gelatin composite scaffolds possessed a highly porous structure with a pore diameter around  $100 \mu\text{m}$ , which was favorable for osteogenic cell ingrowth.<sup>7,33</sup>

Fig. 3A shows the FTIR spectra of the MSNs, Gelatin and MSNs/Gelatin scaffolds (containing 10 wt% MSNs). Compared to MSNs and Gelatin scaffolds, the characteristic peak at  $1071 \text{ cm}^{-1}$  attributed to the Si–O–Si stretching vibration was found in the spectrum of the MSNs/Gelatin scaffold,<sup>34</sup> providing evidence of MSNs incorporated in the composite scaffold. The mechanical property of the tissue engineering scaffold is a key

factor governing the potential application. Thus, compression tests of the composite scaffolds were examined. The characterizations of the mechanical properties of composite scaffolds are shown in Fig. 3B and C. After the incorporation of MSNs, the MSNs/Gelatin composite scaffolds showed an increased compressive modulus *versus* the pure Gelatin scaffold. For example, the compressive modulus of the 5% MSNs/Gelatin sample was  $10.57 \pm 0.35 \text{ MPa}$ , 75.3% higher than that of the Gelatin control ( $6.03 \pm 0.83 \text{ MPa}$ ). Nevertheless, the compressive modulus of the composite scaffolds decreased with a higher MSNs content, but was still as high as  $9.21 \pm 1.07 \text{ MPa}$  when the MSNs content was 20% in the composite scaffolds. Therefore, the results suggested that the addition of MSNs would cause an enhancement in the compression property of the MSNs/Gelatin composite scaffolds. Based on the balance of drug loading capacity and mechanical strength, the 10% MSNs/Gelatin composite scaffolds were used to perform the rest of the studies, unless specified otherwise.

The *in vitro* Van release profile from the Van@MSNs/Gelatin composite scaffold was investigated, and the Van@Gelatin scaffold was included as a control. From Fig. 3D, an obvious burst release of Van from Van@Gelatin was found in the initial

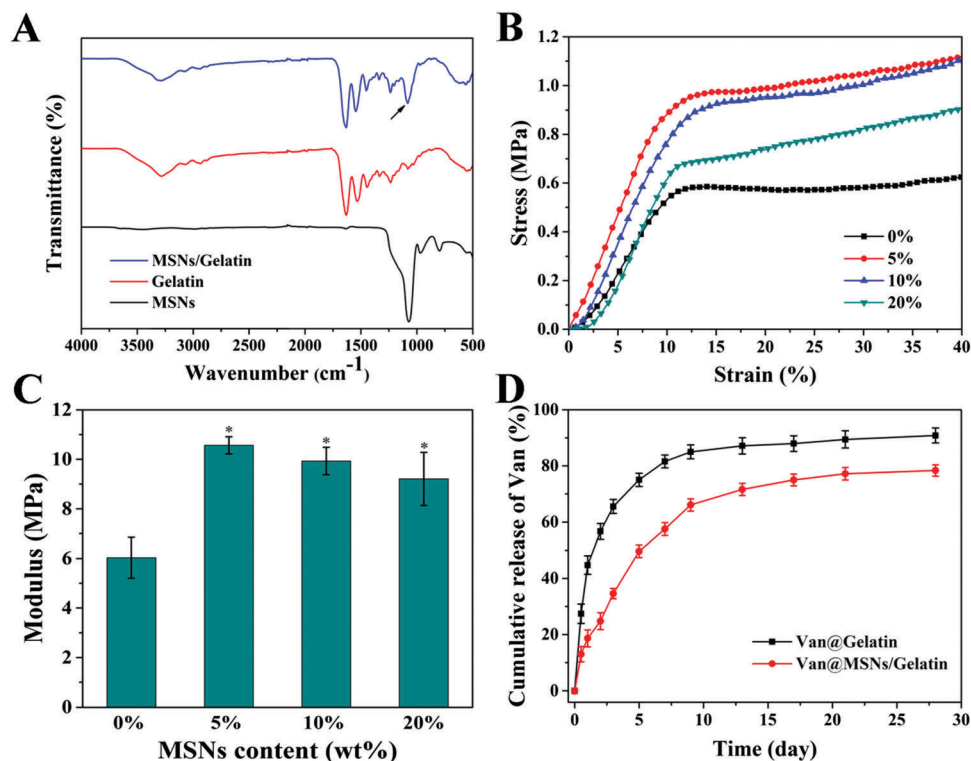


Fig. 3 (A) ATR-FTIR spectra of MSNs, Gelatin and MSNs/gelatin scaffolds. (B) Stress-strain curves of MSNs/Gelatin composite scaffolds with different MSNs contents. (C) Effects of MSNs content on the compression modulus of the MSNs/Gelatin composite scaffolds. (D) The cumulative release profiles of Van from Van@Gelatin and Van@MSNs/Gelatin scaffolds.

stage. The released amount of Van reached up to 45% in the first day, followed by most of the residual drug released within 9 days (around 85% Van released). In contrast, the Van release rate from Van@MSNs/Gelatin was relatively gentle, with an initial fast release and subsequent sustained release pattern. Note that nearly 19% of the loaded Van was released on the 1, and about 78% of Van was released over 28 days. The Van@Gelatin scaffold displayed the fast release of Van due to the fact that Van was located in the gelatin matrix by the physical interaction, which was insufficient to strongly confine the drug release rate. Owing to the protection afforded by the MSNs and polymer matrix,<sup>35</sup> by contrast, the Van@MSNs/Gelatin with a multibarrier structure achieved a reduced release rate and sustained release of Van.

### 3.3 *In vitro* antibacterial activity assay

The Van-loaded composite scaffold was expected to show an effective antibacterial activity. Thus, antibacterial activity experiments with quantitative and qualitative analyses were carried out to validate that the vancomycin was still active after incorporation in the composite scaffolds. As shown in Fig. 4A, the antibacterial activity of Van@Gelatin and Van@MSNs/Gelatin was dose-dependent. Due to the absence of an effective antibacterial ingredient, the Gelatin and MSNs/Gelatin scaffolds did not cause an apparent growth inhibition against *S. aureus*. It was clearly seen that free Van was able to effectively inhibit bacterial growth with more than 94% at the tested

Van concentrations from 10 to 60  $\mu\text{g mL}^{-1}$ . When the drug concentration was 60  $\mu\text{g mL}^{-1}$ , the bacterial inhibition percentages of Van@Gelatin and Van@MSNs/Gelatin both reached 95%, showing no significant difference as compared with free Van. At lower concentrations of Van (20 or 40  $\mu\text{g mL}^{-1}$ ), however, the bacterial inhibition effect of them was dramatically reduced, and Van@Gelatin induced a higher bacterial inhibition percentage than Van@MSNs/Gelatin, which was due to the relatively fast release of Van from Van@Gelatin in the initial period. At a Van concentration of 10  $\mu\text{g mL}^{-1}$ , both Van@Gelatin and Van@MSNs/Gelatin displayed a very low antibacterial effect, with the bacterial inhibition percentage less than 12%, which was attributed to the smaller amount of Van released. To further examine the antibacterial ability of the Van-loaded composite scaffold, an inhibition zone test was performed. As seen in Fig. 4B, obvious inhibition rings were formed surrounding the Van@Gelatin and Van@MSNs/Gelatin scaffolds after 12 and 24 h incubation, indicating that Van released from the scaffold was bioactive against *S. aureus*. The formed inhibition ring on the Van@MSNs/Gelatin scaffold was smaller than that on Van@Gelatin scaffold (Table S2, ESI<sup>†</sup>), which was due to the lower concentration of Van released from the former. In contrast, both the Gelatin and MSNs/Gelatin scaffolds without Van loading did not display a visible inhibitory effect on bacterial growth.

The antibacterial activity of the Van@MSNs/Gelatin scaffold after 3, 7 or 13 days of release was further examined both

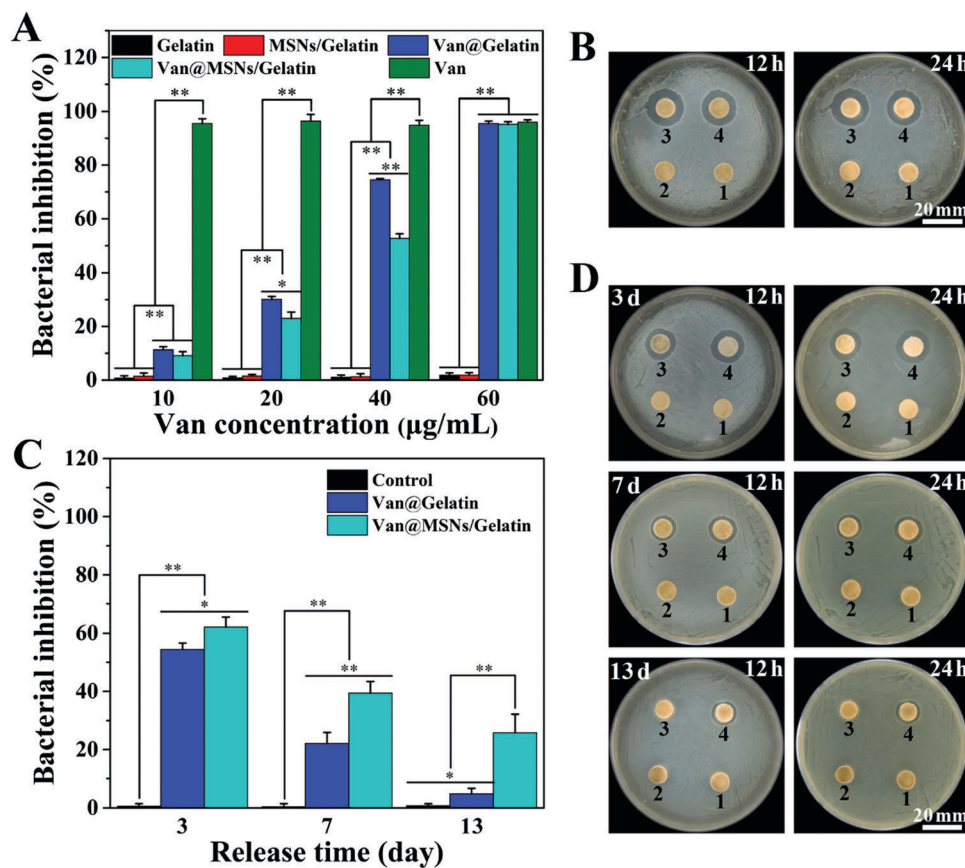


Fig. 4 (A) Growth inhibition of bacteria (*S. aureus*) in a liquid medium after incubation with different samples at various Van concentrations for 24 h. (B) Bacterial growth inhibition on agar plates after 12 and 24 h incubation. (C) Growth inhibition of bacteria in liquid medium after incubation for 24 h using samples (original Van content in each sample was  $60 \mu\text{g mL}^{-1}$  in 5 mL medium and untreated bacterial solution was set as control) after 3, 7 or 13 days release. (D) Bacterial growth inhibition on agar plate after 12 and 24 h incubation using samples after 3, 7 or 13 days release. Numbers 1-4 indicate Gelatin, MSNs/Gelatin, Van@Gelatin and Van@MSNs/Gelatin scaffolds. \* $P < 0.05$ , \*\* $P < 0.01$ .

quantitatively and qualitatively. As shown in Fig. 4C, the bacterial inhibition percentages of Van@Gelatin and Van@MSNs/Gelatin scaffolds were 54.4% and 62.2% after 3 days of release, respectively. However, the antibacterial effect of Van@Gelatin was sharply decreased and was much less effective than that of Van@MSNs/Gelatin after 7 and 13 days of release, which was likely due to the fast loss of loaded Van. After 13 days of release, the bacterial inhibition efficiency of the Van@Gelatin scaffold was only 4.9%, whereas the Van@MSNs/Gelatin scaffold was still able to obtain a bacterial inhibition percentage of 25.8%. From the qualitative antibacterial results in Fig. 4D, both Van@Gelatin and Van@MSNs/Gelatin scaffolds showed visible bacterial inhibition rings after 3 and 7 days of release. But the diameter of the formed inhibition ring for the Van@MSNs/Gelatin scaffold was larger than that for the Van@Gelatin scaffold (Table S3, ESI<sup>†</sup>). After a longer release time (13 days), the inhibition ring for Van@Gelatin scaffold was not obvious, while Van@MSNs/Gelatin scaffold still had significant antibacterial activity. Taken together, these results suggested that Van released from Van@MSNs/Gelatin scaffold still maintained the antibacterial activity, and the sustained release property would yield a long-term antibacterial effect to inhibit bacterial growth.

### 3.4 BMSC proliferation on scaffolds

Before further biomedical applications, the cytocompatibility of the Van@MSNs/Gelatin scaffold was studied. The proliferation of BMSCs on different scaffolds was detected at 2, 4 and 7 days by CCK-8 assay, as shown in Fig. 5A. From the quantitative result, BMSCs cultured on the three scaffolds exhibited a significant increase in cell numbers over the incubation time, indicating good cytocompatibility. There was no significant difference on cell activity among these scaffolds at 2 days and 4 days. After 7 days of incubation, the OD values for both the MSNs/Gelatin and Van@MSNs/Gelatin scaffolds were higher than that of the Gelatin scaffold ( $P < 0.05$ ). The result suggested that the incorporation of MSNs within the scaffold could facilitate cell growth and promote cell proliferation to some extent.<sup>20,21</sup> Additionally, the promoting effect on cell proliferation was not reduced by loading of Van in the scaffold since Van was nontoxic to the cells.<sup>36</sup> The cell morphology and proliferation on the Gelatin, MSNs/Gelatin and Van@MSNs/Gelatin scaffolds were further observed by using live cell imaging. From the fluorescence images in Fig. 5B, all the samples displayed good biocompatibility and were able to support cell attachment with spreading morphology at 2 days. Notably, the cell number

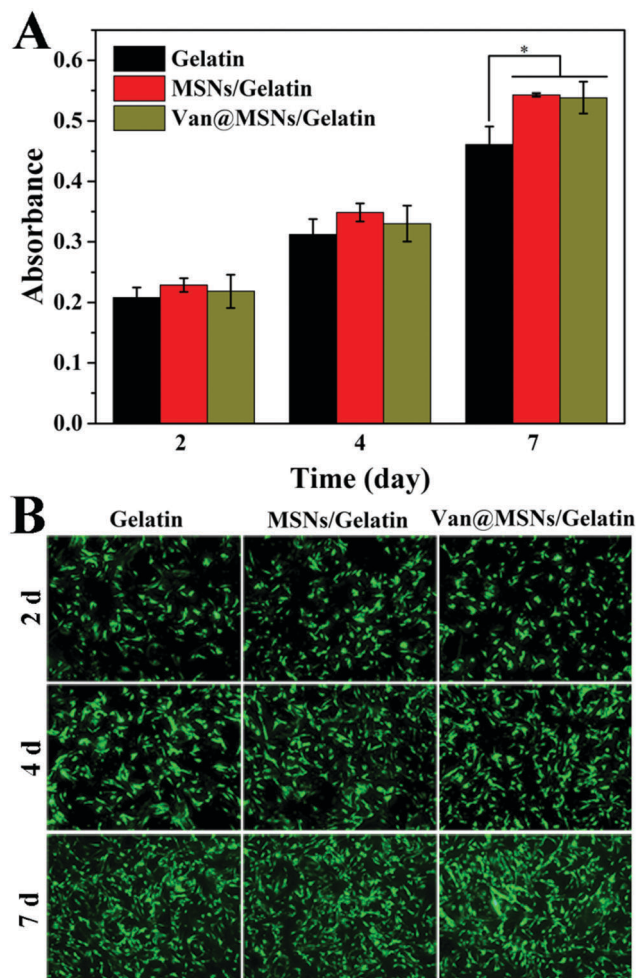


Fig. 5 BMSC proliferation on Gelatin, MSNs/Gelatin and Van@MSNs/Gelatin composite scaffolds for 2, 4 and 7 days. (A) Quantitative analysis by CCK-8 assay and (B) qualitative analysis by live cell staining. The fluorescent images were obtained by the depth of field in the fluorescence microscope, magnification: 100 $\times$ .

on the scaffolds increased gradually with culture time. At day 7, more live cells had grown on the scaffolds. Overall, the Van@MSNs/Gelatin scaffold had a good cytocompatibility to allow cell spreading and proliferation.

### 3.5 Osteogenic differentiation *in vitro*

To determine whether the Van-loaded MSNs/Gelatin composite scaffold was appropriate for bone regeneration, the ALP, regarded as a significant osteogenic marker, was first measured. From Fig. 6A, the increase in ALP activity was observed in each group after a longer culture time, indicating the osteogenic differentiation of BMSCs when cultured under the induction medium. At 7 days of culture, it was found that there were no significant differences in the ALP activity among the groups. However, BMSCs cultured on the MSNs/Gelatin and Van@MSNs/Gelatin scaffolds showed a higher level of ALP than those cultured on the Gelatin scaffold after 14 days of osteogenic culture, while there was no significant difference between the MSNs/Gelatin and Van@MSNs/Gelatin scaffolds. We also analyzed the gene

expression of osteogenic markers, including RUNX2, OPN and OCN (Fig. 6B–D). RUNX2 acts as one of the earliest indicators of osteogenic differentiation, and belongs to RUNX family.<sup>37</sup> As the master regulator during osteogenesis, it is essential in regulating the expression of downstream osteo-related genes like OPN and OCN. The expression of these genes was enhanced from day 7 to day 14 for the Gelatin, MSNs/Gelatin and Van@MSNs/Gelatin groups. In contrast with the cells cultured on the Gelatin scaffold, the mRNA expression of RUNX2 significantly increased in cells cultured on the composite scaffolds at day 7. In addition, the mRNA expression level of OCN in both the MSNs/Gelatin and Van@MSNs/Gelatin groups were higher than on the Gelatin group after 14 days of incubation. Similarly, no significant difference on the expression of these marker genes was observed between MSNs/Gelatin and Van@MSNs/Gelatin. Thus, the results suggested that the incorporation of MSNs in the scaffold showed the ability to facilitate the osteogenic differentiation of BMSCs, and Van loading has no obvious negative effects on its bioactivity. In recent years, silica nanoparticles have been widely studied and demonstrated to enhance osteoblastic differentiation,<sup>38,39</sup> and their biological activity still remained after being incorporated into the polymer matrix.<sup>4,21</sup> Furthermore, recent evidence also suggested that the deposition of MSNs on the polymer scaffold also led to an increase in osteogenic marker expression and promoted the mineralized matrix formation.<sup>17</sup>

### 3.6 Regeneration of infected bone defects

To determine whether Van@MSNs/Gelatin was suitable for the treatment of infected bone defects, an infected bone defect model in the rabbit radius was established for further evaluation. Prior to implantation of the as-prepared scaffolds in the defect sites, the established infected models were verified. From the digital photograph of the surgical wound in the animal model, pus was discharging from the wound at two weeks post-operation (Fig. S3A, ESI<sup>†</sup>), which indicated that the infection and inflammatory response happened in the defect site. Notably, the WBC concentrations of all the groups were sharply increased and reached a peak at day 7, thereafter followed by a slight decline (Fig. S3B, ESI<sup>†</sup>). At day 14, however, they were significantly elevated as compared to the initial level (~2-fold) due to the deficiency of antibiotics. Additionally, the infected sample was infiltrated with bacteria among the necrotic bone trabeculae in Gram stained sections (Fig. S4A, ESI<sup>†</sup>). Furthermore, the Masson's trichrome stained sections showed the damaged bone trabeculae with impaired morphology (Fig. S4B, ESI<sup>†</sup>). Therefore, these results revealed the successful establishment of the infected bone defect model.

Before scaffold implantation, debridement was applied in the wound. Following this step, the scaffolds were respectively implanted into the defects. We also monitored the WBC concentrations weekly after scaffold implantation (Fig. 7). It was noted that the WBC concentrations still remained at a high level after 8 weeks in both the Gelatin and MSNs/Gelatin groups due to the deficiency of efficacious antibiotics. In contrast, the WBC concentration decreased significantly after implantation in the

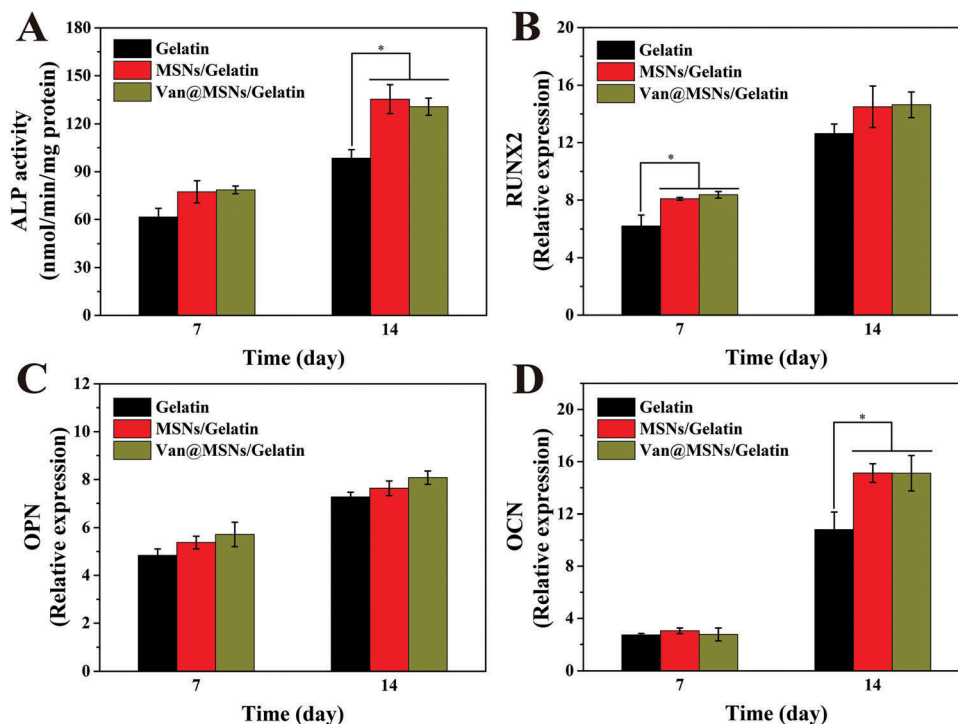


Fig. 6 *In vitro* osteogenic differentiation evaluation of BMSCs cultured on the Gelatin, MSNs/Gelatin and Van@MSNs/Gelatin scaffolds for 7 and 14 d. (A) ALP activity, osteo-related gene, (B) RUNX2, (C) OPN and (D) OCN expression. \* $P < 0.05$ .

Van@MSNs/Gelatin group, and eventually recovered to its normal level at 4 weeks post-implantation, which was mainly attributed to the controlled release of Van from the well-designed drug delivery system. Along with the introduction of a local drug delivery strategy into bone repair implants, the controlled release concept became widely accepted in bone infection treatment and recurrence prevention owing to its merits in elevating local concentrations and extending the antibacterial duration. Accordingly, this result confirmed that the Van@MSNs/Gelatin scaffold with a controlled release of Van had an effective antibacterial activity to inhibit local infection *in vivo*.

The collected specimens were subsequently scanned using a micro-CT to evaluate the repair capacity of different implants. From the reconstructed 3D micro-CT images in Fig. 8A, the difference in bone regeneration rate among the groups can be detected. At 4 weeks post-implantation, there was no obvious new bone formation in the Gelatin group. However, a small amount of opaque tissue could be observed at the defect sites for the MSNs/Gelatin and Van@MSNs/Gelatin groups. At 8 weeks post-implantation, new bone formation was visible in all groups. It was noted that the regenerated bone mainly appeared at the two ends of the defect sites in the Gelatin group and MSNs/Gelatin group. For the Van@MSNs/Gelatin group, partial fusion of the new bone was observed in the defect area, which implied a superior bone repair efficiency. Furthermore, the Van@MSNs/Gelatin group also showed more new bone at 12 weeks when compared to the other groups. Specifically, we found that a complete bony bridge presented in the Van@MSNs/Gelatin

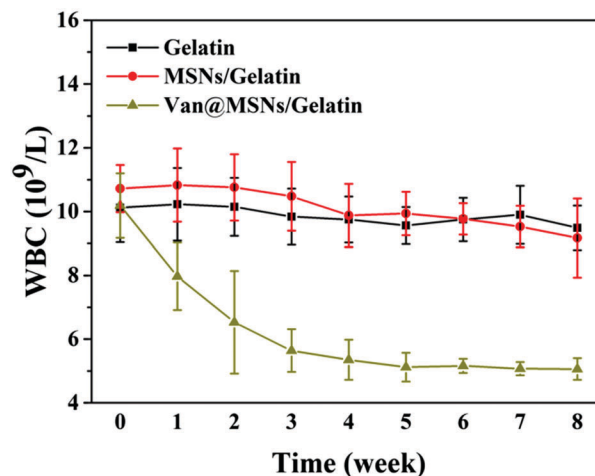


Fig. 7 WBC determination at different time points after Gelatin, MSNs/Gelatin, Van@MSNs/Gelatin scaffold implantation.

group. The generated bone volume and bone mineral density were also measured for a quantitative analysis of bone formation (Fig. 8B and C). From 4 to 12 weeks, the bone volumes were significantly increased in all three groups. Compared with the other two groups, the Van@MSNs/Gelatin group demonstrated significantly higher values of bone volume at each time point. On the other hand, the bone mineral density value of this group was also higher than that of the other two groups. These results demonstrated that Van@MSNs/Gelatin could efficiently promote bone healing in infected bone defects owing to the sustained

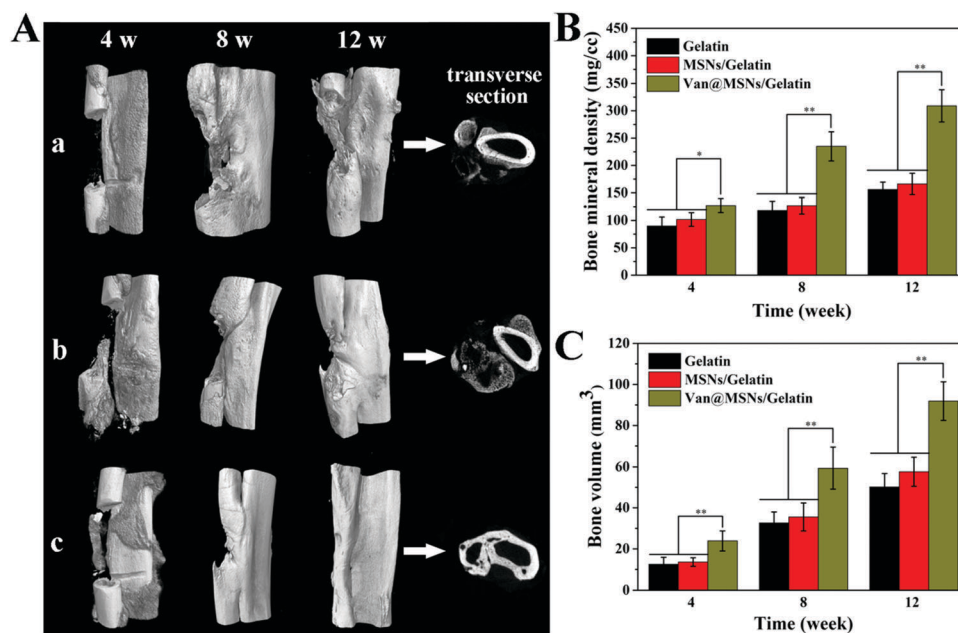


Fig. 8 (A) 3D micro-CT reconstructed images of rabbit radii at 4, 8, and 12 weeks with different implants: (a) Gelatin, (b) MSNs/Gelatin and (c) Van@MSNs/Gelatin scaffolds. Quantitative analysis of regenerated (B) bone mineral density and (C) bone volume at 4, 8 and 12 weeks. \* $P < 0.05$ , \*\* $P < 0.01$ .

release of the antibiotic, while the dissatisfactory outcomes in the Gelatin and MSNs/Gelatin groups were attributed to bacterial contamination. Although the scaffold with a porous structure encouraged new bone formation *via* an efficient cell ingrowth,<sup>4</sup> the infection and inflammation that results from the bacteria invasion would seriously hinder new bone formation during bone healing.<sup>40</sup>

The histological evaluations were performed to further compare the repair performance of these implants, including H&E and T-blue staining (Fig. 9). The representative H&E stained sections are shown in Fig. 9A. Obviously, the contamination in the osseous tissues remained unquenched for Gelatin and MSNs/Gelatin groups at 8 and 12 weeks, where there was visible inflammatory cell infiltration. In comparison, the infection was significantly reduced in the Van@MSNs/Gelatin group and there were more densely regenerated bone trabeculae with a thicker and intact morphology until 12 weeks after implantation. Similarly, the T-blue stained sections also showed a better bone formation in the Van@MSNs/Gelatin group (Fig. 9B). Furthermore, the Van groups were carried out as controls which were administered in two ways (Fig. S5, ESI†). The results exhibited that the local injection of Van (Control 1) also displays unsatisfactory bone formation at 12 weeks, which may result from the rapid loss of antibiotics and short-term inhibition on bacterial growth.<sup>41</sup> The animals treated by the intravenous injection of Van (Control 2) showed that the regenerated bone was dramatically increased, whereas the bone quality was not as good as that of the Van@MSNs/Gelatin group and obvious contamination could be observed from the histological results. Here, no significant differences on the bone formation between the Gelatin and MSNs/Gelatin groups were observed. Although *in vitro* studies had demonstrated the

enhanced osteogenic property of the MSNs-incorporated scaffold, we speculated that this positive function was dramatically restrained by bacterial contamination. Therefore, the above results further confirmed that the Van@MSNs/Gelatin with a locally controlled release of antibiotic exhibited a better performance on bone formation in contaminated bone defects.

In the present study, this is the first time that a Van-loaded MSNs/Gelatin composite scaffold was fabricated for the treatment of infected bone defects. From the literature, most of the prepared gelatin-based porous scaffolds showed that the pores were distorted and pore shells were clogged partially.<sup>23,42,43</sup> By contrast, the fabricated MSNs/Gelatin composite scaffolds in this study showed a homogeneous and well-defined pore structure with highly open-channeled macropores and an interconnected framework, which might be attributed to a gradient cooling process before lyophilization. Furthermore, the addition of MSNs led to an increase in the pore size, making the scaffolds more appropriate for vascularization and tissue ingrowth in bone tissue engineering. With the incorporation of MSNs, the Van@MSNs/Gelatin composite scaffold revealed a better controlled release of Van and displayed a significantly reduced initial release, which eventually presented a long-term effective inhibition effect on bacterial growth as evidenced by an *in vitro* antibacterial activity evaluation. Finally, a delightful outcome of infected bone defect therapy was achieved in the animal studies as the prepared composite scaffold could simultaneously provide effective infection control and structural support for bone tissue ingrowth. Thus, through a systemic study, our results revealed that a MSNs-incorporated gelatin scaffold could be used for local antibacterial drug delivery and infected bone defect treatment.

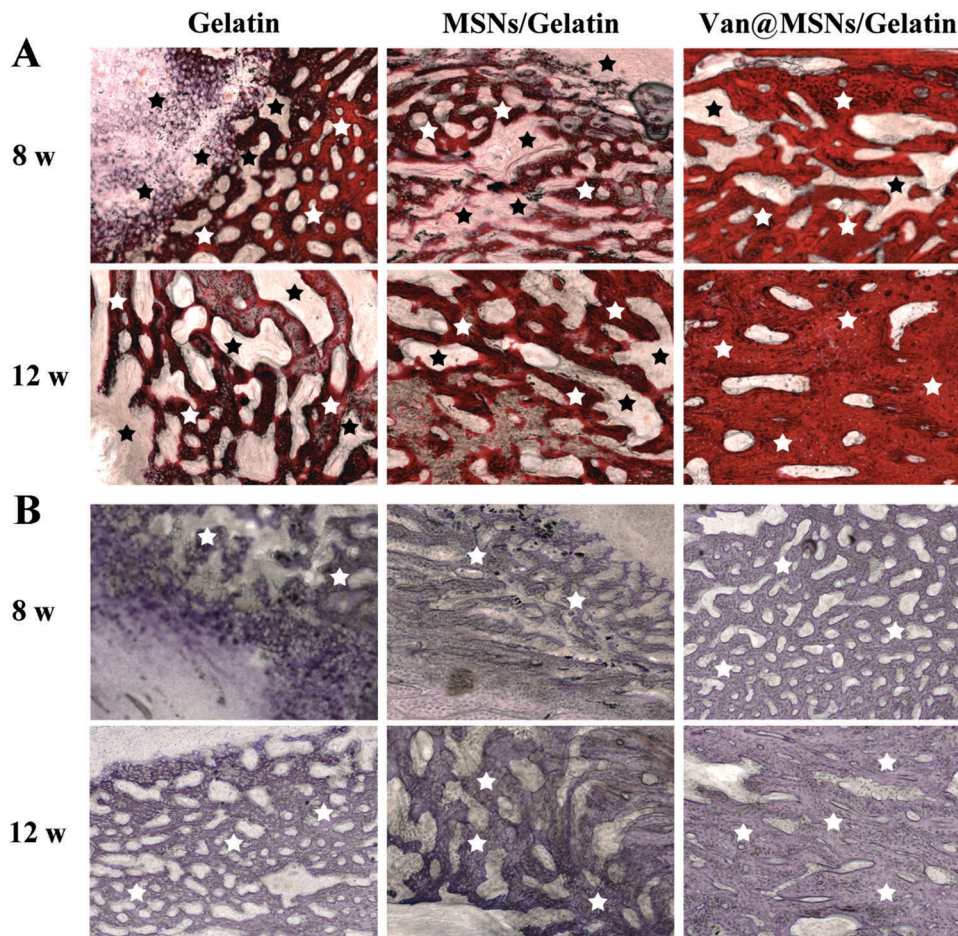


Fig. 9 Histological evaluation of bone defect repair after implantation with Gelatin, MSNs/Gelatin and Van@MSNs/Gelatin scaffolds for 8 and 12 weeks. (A) H&E staining and (B) T-blue staining. Black stars indicate the inflammatory cells and white stars indicate the newly formed bone.

## 4. Conclusions

In this study, the Van@MSNs/Gelatin composite scaffold was fabricated by the integration of a gelatin matrix and Van-loaded MSNs for the treatment of infected bone defects. The gelatin-based three-dimensional scaffolds with a highly interconnected porous structure were demonstrated. By the addition of MSNs, the compressive properties of the composite scaffolds were improved, significantly higher than that of the Gelatin scaffold. In addition, the introduction of MSNs endowed the composite scaffold with a better cell proliferation, as well as an enhanced osteogenic property. Owing to the sustained release manner of the loaded antibiotic, the Van@MSNs/Gelatin scaffold exhibited significant antibacterial activity both *in vitro* and *in vivo*. Most importantly, the Van@MSNs/Gelatin scaffold was capable of achieving an improved bone regeneration in contaminated bone defects, suggesting that it might be identified as a promising repair material for infected bone defects.

## Conflicts of interest

There are no conflicts to declare.

## Acknowledgements

This work was financially supported by the National Natural Science Foundation of China (31771048, 31570984, 31271028, 81702124), and the International Cooperation Fund of the Science and Technology Commission of Shanghai Municipality (15540723400).

## Notes and references

- 1 E. N. Johnson, T. C. Burns, R. A. Hayda, D. R. Hospenthal and C. K. Murray, *Clin. Infect. Dis.*, 2007, **45**, 409–415.
- 2 W. T. Jia, Q. Fu, W. H. Huang, C. Q. Zhang and M. N. Rahaman, *Antimicrob. Agents Chemother.*, 2015, **59**, 7571–7580.
- 3 Z. Xie, X. Liu, W. Jia, C. Zhang, W. Huang and J. Wang, *J. Controlled Release*, 2009, **139**, 118–126.
- 4 S. Zhang, Y. Guo, Y. Dong, Y. Wu, L. Cheng, Y. Wang, M. Xing and Q. Yuan, *ACS Appl. Mater. Interfaces*, 2016, **8**, 13242–13250.
- 5 M. A. Rauschmann, T. A. Wichelhaus, V. Stiral, E. Dingeldein, L. Zichner, R. Schnettler and V. Alt, *Biomaterials*, 2005, **26**, 2677–2684.

- 6 Z. Cao, D. Jiang, L. Yan and J. Wu, *J. Biomater. Appl.*, 2016, **30**, 1566–1577.
- 7 F. Chen, Z. Song, L. Gao, H. Hong and C. Liu, *J. Mater. Chem. B*, 2016, **4**, 4198–4205.
- 8 W. Weng, W. Nie, Q. Zhou, X. Zhou, L. Cao, F. Ji, J. Cui, C. He and J. Su, *RSC Adv.*, 2017, **7**, 2753–2765.
- 9 B. Li, K. V. Brown, J. C. Wenke and S. A. Guelcher, *J. Controlled Release*, 2010, **145**, 221–230.
- 10 M. Zilberman and J. J. Elsner, *J. Controlled Release*, 2008, **130**, 202–215.
- 11 J. Zhou, T. Fang, Y. Wang and J. Dong, *J. Biomed. Mater. Res., Part A*, 2012, **100**, 2295–2301.
- 12 J. Gu, T. Wang, G. Fan, J. Ma, W. Hu and X. Cai, *J. Mater. Sci.: Mater. Med.*, 2016, **27**, 1–11.
- 13 J. H. Lee, A. El-Fiqi, J. K. Jo, D. A. Kim, S. C. Kim, S. K. Jun, H. W. Kim and H. H. Lee, *Dent. Mater.*, 2016, **32**, 1564–1574.
- 14 Q. Wang, C. Chen, W. Liu, X. He, N. Zhou, D. Zhang, H. Gu, J. Li, J. Jiang and W. Huang, *Sci. Rep.*, 2017, **7**, 41808.
- 15 P. Gentile, V. K. Nandagiri, J. Daly, V. Chiono, C. Mattu, C. Tonda-Turo, G. Ciardelli and Z. Ramtoola, *Mater. Sci. Eng., C*, 2016, **59**, 249–257.
- 16 F. Zheng, S. Wang, S. Wen, M. Shen, M. Zhu and X. Shi, *Biomaterials*, 2013, **34**, 1402–1412.
- 17 K. Qiu, B. Chen, W. Nie, X. Zhou, W. Feng, W. Wang, L. Chen, X. Mo, Y. Wei and C. He, *ACS Appl. Mater. Interfaces*, 2016, **8**, 4137–4148.
- 18 X. Zhou, W. Feng, K. Qiu, L. Chen, W. Wang, W. Nie, X. Mo and C. He, *ACS Appl. Mater. Interfaces*, 2015, **7**, 15777–15789.
- 19 L. Chen, X. Zhou, W. Nie, Q. Zhang, W. Wang, Y. Zhang and C. He, *ACS Appl. Mater. Interfaces*, 2016, **8**, 33829–33841.
- 20 M. Mehra, M. A. Asadollahi, B. Nasri-Nasrabadi, K. Ghaedi, H. Salehi, A. Dolatshahi-Pirouz and A. Arpanaei, *Mater. Sci. Eng., C*, 2016, **66**, 25–32.
- 21 K. Li, H. Sun, H. Sui, Y. Zhang, H. Liang, X. Wu and Q. Zhao, *RSC Adv.*, 2015, **5**, 17541–17549.
- 22 B. Song, C. Wu and J. Chang, *Acta Biomater.*, 2012, **8**, 1901–1907.
- 23 H. W. Kim and K. H. E. Kim, *J. Biomed. Mater. Res., Part B*, 2005, **74B**, 686–698.
- 24 J. Li, Y. Chen, Y. Yin, F. Yao and K. Yao, *Biomaterials*, 2007, **28**, 781–790.
- 25 C. Sharma, A. K. Dinda, P. D. Potdar, C. F. Chou and N. C. Mishra, *Mater. Sci. Eng., C*, 2016, **64**, 416–427.
- 26 M. C. Echave, P. Sánchez, J. L. Pedraz and G. Orive, *J. Drug Delivery Sci. Technol.*, 2017, **42**, 63–74.
- 27 F. J. Martínez-Vázquez, M. V. Cabañas, J. L. Paris, D. Lozano and M. Vallet-Regí, *Acta Biomater.*, 2015, **15**, 200–209.
- 28 M. Yamamoto, A. Hokugo, Y. Takahashi, T. Nakano, M. Hiraoka and Y. Tabata, *Biomaterials*, 2015, **56**, 18–25.
- 29 C. Wang, H. Shen, Y. Tian, Y. Xie, A. Li, L. Ji, Z. Niu, D. Wu and D. Qiu, *ACS Appl. Mater. Interfaces*, 2014, **6**, 13061–13068.
- 30 M. Yazdimamaghani, D. Vashae, S. Assefa, K. J. Walker, S. V. Madihally, G. A. Köhler and L. Tayebi, *J. Biomed. Nanotechnol.*, 2014, **10**, 911–931.
- 31 X. Cui, C. Zhao, Y. Gu, L. Li, H. Wang, W. Huang, N. Zhou, D. Wang, Y. Zhu and J. Xu, *J. Mater. Sci.: Mater. Med.*, 2014, **25**, 733–745.
- 32 X. Li, B. Shi, Y. Wang, M. Li, Y. Liu, L. Gao and L. Mao, *Microporous Mesoporous Mater.*, 2015, **214**, 15–22.
- 33 K. Rezwani, Q. Chen, J. Blaker and A. R. Boccaccini, *Biomaterials*, 2006, **27**, 3413–3431.
- 34 X. Zhou, X. Cheng, W. Feng, K. Qiu, L. Chen, W. Nie, Z. Yin, X. Mo, H. Wang and C. He, *Dalton Trans.*, 2014, **43**, 11834–11842.
- 35 L. Li, G. Zhou, Y. Wang, G. Yang, S. Ding and S. Zhou, *Biomaterials*, 2015, **37**, 218–229.
- 36 L. Zhang, J. Yan, Z. Yin, C. Tang, Y. Guo, D. Li, B. Wei, Y. Xu, Q. Gu and L. Wang, *Int. J. Nanomed.*, 2014, **9**, 3027–3036.
- 37 T. M. Liu and E. H. Lee, *Tissue Eng., Part B*, 2012, **19**, 254–263.
- 38 G. R. Beck, S. W. Ha, C. E. Camalier, M. Yamaguchi, Y. Li, J. K. Lee and M. N. Weitzmann, *Nanomedicine*, 2012, **8**, 793–803.
- 39 M. Shi, Y. Zhou, J. Shao, Z. Chen, B. Song, J. Chang, C. Wu and Y. Xiao, *Acta Biomater.*, 2015, **21**, 178–189.
- 40 M. Simion, P. Trisi, M. Maglione and A. Piattelli, *J. Periodontol.*, 1994, **65**, 755–761.
- 41 L. Gang, C. Si, J. Fang, B. Xu, L. Shuang, Y. Hao, N. A. Aldhabi, S. Deng and V. Duraipandiyar, *BMC Pharmacol. Toxicol.*, 2016, **17**, 61.
- 42 K. C. Kavya, R. Jayakumar, S. Nair and K. P. Chennazhi, *Int. J. Biol. Macromol.*, 2013, **59**, 255–263.
- 43 I. R. Serra, R. Fradique, M. C. Vallejo, T. R. Correia, S. P. Miguel and I. J. Correia, *Mater. Sci. Eng., C*, 2015, **55**, 592–604.